

# The optical properties of cermets from the theory of electrostatic resonances†

Y Kantor and D J Bergman

Department of Physics and Astronomy, Tel Aviv University, Tel Aviv, 69978, Israel

Received 8 July 1981

**Abstract.** A recently developed exact theory of electrostatic resonances in two-component composite materials is applied to the discussion of optical properties of some cermets (ceramic–metal mixtures). A considerable improvement in the agreement with experiments is achieved as compared with the effective-medium and Maxwell-Garnett approximations.

## 1. Introduction

Granular metals are a very interesting class of composite materials. They are prepared either as cermets (ceramic–metal mixtures), as discontinuous thin metal films, or as metal smokes. The unusual optical properties of these systems have been investigated both experimentally and theoretically, for example, in the case of cermets Ag, Au or Mg embedded in SiO<sub>2</sub> or MgF<sub>2</sub> matrices (Cohen *et al* 1973, Sichel and Gittelman 1977, Lissberger and Nelson 1974), in the case of discontinuous Ag, Au or Cr films (Norman *et al* 1978, O'Neill and Ignatiev 1978, Doremus 1964, 1965, Ignatiev *et al* 1979, Granqvist *et al* 1979, Jarrett and Ward 1976) and in the case of Al, Cu and Sn smokes (Tanner *et al* 1975, Granqvist *et al* 1976).

Granular metals are usually investigated by measuring the optical density (i.e.,  $-\lg T$ , where  $T$  is the transmission factor) of a particular sample. One of the most striking features in the optical properties is a strong absorption peak in the visible region. The precise location of this peak depends upon the dielectric properties of the components, as well as on the microgeometry of the mixture.

The optical transmission, as well as the other optical properties, is determined by the complex effective dielectric constant of the mixture  $\epsilon_e$ . One of the oldest theoretical estimates of  $\epsilon_e$  is the Maxwell-Garnett equation (Maxwell-Garnett 1904, 1905) (see equation (16)). This equation predicts quite well the location, but not the height, of the absorption peak in granular metals. Maxwell-Garnett theory (MGT), which treats one of the components as the medium and the other as inclusions, is a nonsymmetric theory. By contrast, the effective medium theory (EMT) (Bruggeman 1935, Landauer 1952) treats both components symmetrically. However in many cases it fails to predict the absorption peak that is observed in the granular metals (see, e.g., Gittelman and Abeles 1977).

† Partially supported by the United States–Israel Binational Science Foundation under grant number 2006/79.

A recent attempt to obtain a more symmetric theory has been made by Sheng (1980a, b). That theory is essentially an effective medium theory where each component is already in the form of composite spheres. The composition and volume fractions of the two components are found by assuming a certain model for the formation process of the composite. This makes the treatment rather specialised, but seems to give good agreement with experiment for a certain class of cermets.

In this article, we take a different approach to this problem based upon a recently developed exact theory for calculating  $\epsilon_e$  for composites where the microgeometry is known precisely (Bergman 1978, 1979a, b). This is in contrast with the approximate theories, which take into account only the lowest order (dipole-dipole) interactions between different inclusions, and therefore fail when the concentrations are large and when the frequency of the light is close to the resonant frequencies of the sample. The approximations that are made when we apply the exact theory of random mixtures do not restrict us to lowest-order interactions between inclusions, and they may in fact be improved in a systematic way, if necessary.

It is important to keep in mind that the theory we are using is exact only in the static limit. Its use in the discussion of the optical properties of a composite is only justified if the sizes of the grains or of other characteristic inhomogeneities are much smaller than both the wavelength and the skin depth in the composite.

The details of the model and of the calculation, as well as a comparison between our results and those of MGT and EMT, are given in § 2. In § 3 we compare the theoretical predictions of MGT, EMT and our model with experiments. In § 4 we summarise the results and compare the main features of our model with other theories.

## 2. Calculation of $\epsilon_e$

The position dependent local dielectric constant of a two-component mixture can be written in the following form:

$$\epsilon(\mathbf{r}) = \epsilon_2[1 - (1/s)\theta(\mathbf{r})] \quad (1)$$

where

$$\theta(\mathbf{r}) \equiv \begin{cases} 1, & \text{for } \mathbf{r} \text{ inside } \epsilon_1\text{-material} \\ 0, & \text{for } \mathbf{r} \text{ outside } \epsilon_1\text{-material} \end{cases} \quad (2)$$

$$s \equiv \epsilon_2/(\epsilon_2 - \epsilon_1). \quad (3)$$

We now summarise the main results of the exact theory for the calculation of  $\epsilon_e$  in the static limit (Bergman 1978, 1979a, b).

The bulk effective dielectric constant  $\epsilon_e$  can be expressed in terms of the electrostatic resonances of the composite in the following form:

$$F(s) \equiv 1 - \frac{\epsilon_e}{\epsilon_2} = \frac{1}{V} \sum_n \frac{|\langle z | \psi_n \rangle|^2}{s - s_n} \equiv \sum_n \frac{F_n}{s - s_n}. \quad (4)$$

Here the poles  $s_n$  represent special values of  $s(\epsilon_1, \epsilon_2)$  for which an internal electric field can exist in the sample without the application of an external field, the state  $|\psi_n\rangle$  represents the potential field distribution in such a resonance, and the scalar product of any two states (i.e., potential fields in the composite) is defined by:

$$\langle \varphi | \psi \rangle \equiv \int dV \theta(\mathbf{r}) (\nabla \varphi^* \cdot \nabla \psi). \quad (5)$$

(Note that the integration is confined to the  $\epsilon_1$ -volume.) Clearly, all the residues in equation (4) are positive, and furthermore the values of  $s_n$  and  $F_n$  satisfy

$$0 \leq s_n \leq 1 \quad 0 \leq F_n \leq 1. \tag{6}$$

We note that since the resonances are completely determined by the microgeometry, the expansion of equation (4), which has the form of a spectral representation, completely separates the dependence of  $\epsilon_e$  on the geometry of the mixture from its dependence on the physical properties of the components: the locations  $s_n$  and the weights  $F_n$  of the poles depend only on the microgeometry, while the dielectric constants of the components enter only through the variable  $s$ . The resonances can be found by solving the eigenvalue problem of a certain linear hermitian integral operator  $\Gamma$ :

$$s_n \psi_n = \Gamma \psi_n \tag{7}$$

$$\Gamma \psi \equiv \frac{1}{4\pi} \int dV' \theta(\mathbf{r}') \nabla' \cdot \frac{1}{|\mathbf{r} - \mathbf{r}'|} \cdot \nabla' \psi(\mathbf{r}'). \tag{8}$$

For a specified microgeometry in a finite total volume, a set of discrete eigenvalues is found. For a composite with a periodic structure, although continuous bands of eigenvalues are found, only those corresponding to  $\mathbf{k} = 0$  Bloch states contribute to the sum in equation (4), and these are again a discrete set. In the case of a composite with a random geometry, represented by a suitable ensemble, the functions  $F(s)$  must be averaged over the ensemble, and this leads to a smearing of the pole spectrum into a branch cut. (A branch cut is also obtained when the total volume is infinite and the system is disordered.) The ensemble averaged function  $F(s)$  is now represented by:

$$F(s) = \int_{x_1}^{x_2} \frac{f(x)}{s - x} dx \tag{9a}$$

$$f(x) \geq 0, \quad 0 \leq x_1 \leq x_2 \leq 1 \tag{9b}$$

where  $f(x)$ ,  $x_1$ ,  $x_2$  depend only on the statistics of the microgeometry.

We consider the following model: a set of  $N$  spheres with randomly chosen radii  $a_1, \dots, a_N$  are placed at random positions, but without overlapping, in a cubic cell. That cell is then repeated infinitely many times in all directions. In this way we obtain a periodic simple cubic composite, with a random unit cell. The location of each cell is defined by  $\mathbf{R}_0 = (n_1b, n_2b, n_3b)$  where  $b$  is the lattice spacing and the  $n$  are integers. The eigenstates of a single spherical grain and the matrix elements of  $\Gamma$  between the states of different grains (these matrix elements are essentially overlap integrals between states on different grains) were calculated by Bergman (1979a). The eigenstates of such a grain, whose angular dependence is always given by a spherical harmonic, are characterised by the usual angular momentum quantum numbers  $l(=1, 2, \dots)$ ,  $m(= -l, \dots, +l)$ . The matrix element between the state  $(l, m)$  of a sphere of radius  $a$  and the state  $(l', m')$  of another sphere of radius  $a'$  is given by

$$(-1)^{l+m} a^{l+\frac{1}{2}} a'^{l'+\frac{1}{2}} \left( \frac{l!}{(2l+1)(2l'+1)(l+m)!(l-m)!(l'+m')!(l'-m')!} \right)^{1/2} \times (l+l'+m-m')! \frac{P_{l+l'}^{m'-m}(\cos \theta) \exp[i(m'-m)\varphi]}{r^{l+l'+1}} \tag{10}$$

where  $(r, \theta, \varphi)$  is the vector separation of the two centres in spherical coordinates and

$P_L^M$  is an associated Legendre polynomial†. If the  $R = 0$  Bloch states are expanded in a series of the individual sphere eigenstates the coefficients must satisfy an eigenvalue equation whose matrix elements are

$$Q_{ilm,jl'm'} = (-1)^{l'+m'} a_i^{l'+\frac{1}{2}} a_j^{l'+\frac{1}{2}} \left( \frac{l'}{(2l+1)(2l+1)(l+m)!(l-m)!(l'+m')!(l'-m')!} \right)^{1/2} \\ \times \left( \sum_{\lambda=0}^{\infty} \sum_{\mu=-\lambda}^{\lambda} (-1)^{\lambda+\mu} \frac{r^\lambda P_\lambda^\mu(\cos \theta) e^{i\mu\varphi}}{(\lambda+\mu)!} \right) \\ \times (l+l'+\lambda - |m'-m-\mu|)! \sigma(l+l'+\lambda, |m'-m-\mu|) \\ + (l+l'-m'+m)! \frac{P_{l+l'}^{m'-m}(\cos \theta) \exp[i(m'-m)\varphi]}{r^{l+l'+1}}, \quad \text{for } i \neq j \quad (11)$$

$$Q_{ilm,il'm'} = (-1)^{l'+m'} a^{l'+l'+1} \left( \frac{l'}{(2l+1)(2l'+1)(l+m)!(l-m)!(l'+m')!(l'-m')!} \right)^{1/2} \\ \times (l+l' - |m-m'|)! \sigma(l+l', |m-m'|) + \frac{l}{2l+1} \delta_{ll'} \delta_{mm'} \quad (12)$$

where

$$\sigma(L, M) \equiv \sum_{R_0 \neq 0} \frac{P_L^M(\cos \theta_0) \exp(iM\varphi_0)}{R_0^{L+1}} \quad (13)$$

and where the last sum is over all the non-zero lattice vectors of a simple cubic lattice. In these equations, the indices  $i$  and  $j$  denote two spheres in the unit cell, whose radii are  $a_i$  and  $a_j$ , and whose separation is  $(r, \theta, \varphi)$ . The summation over different unit cells is performed in equation (13). The sums in equation (11) appear when the matrix elements of (10) between non-equivalent spheres are summed over all unit cells. The derivation of (11) from (10) is described in detail in the Appendix. The properties of  $\sigma(L, M)$ , as well as some problems in the calculation of  $\sigma(2, 0)$  were discussed by Bergman (1979a).

In our calculation 4 spheres were placed in the repeated cubic cell. The random configurations were generated by computer. For each concentration  $p$  of the first material, the poles and their weights were calculated for 60 different configurations. All of these poles were then superimposed, and a continuous distribution  $f(x)$  was obtained in the form of a histogram with  $\Delta x = 0.02$ . In calculating the pole spectrum for each sample, the matrices were truncated at  $l = l' = 2$ , i.e., only the strongest (dipole and quadrupole) overlaps were taken into account. These results of the calculations of  $f(x)$  for 3 different concentrations are depicted in figure 1. As  $f(x)$  depends only on the microgeometry of the sample, these histograms can now be used to calculate  $\epsilon_e$  for any  $\epsilon_1$  and  $\epsilon_2$ . For comparison, we show the predictions of MGT and EMT for  $f(x)$  in the same figure. In these approximations,  $f(x)$  is given by

$$f(x)_{\text{MGT}} = p\delta[x - \frac{1}{3}(1-p)] \quad (14)$$

$$f(x)_{\text{EMT}} = \begin{cases} \frac{1}{4\pi x} (-9x^2 + 6(1+p)x - (1-3p)^2)^{1/2}, & \text{for } x_1 \leq x \leq x_2 \\ 0, & \text{otherwise} \end{cases} \quad (15a)$$

† For  $M < 0$ , we use the following convention for  $P_L^M$  (see e.g., Messiah 1962)

$$P_L^M = (-1)^M \frac{(L+M)!}{(L-M)!} P_L^{-M}$$

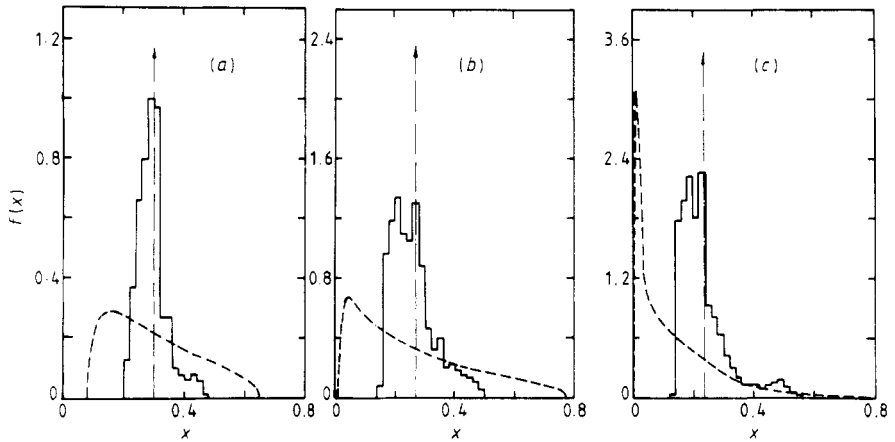


**Figure 1.** Pole density function  $f(x)$  for 3 different concentrations (a)  $p = 0.1$ , (b)  $p = 0.2$ , (c)  $p = 0.3$  as predicted by EMT (broken curve), MGT (chain vertical line represents a  $\delta$ -function) and our calculation (full line-histogram).

$$x_{1,2} = \frac{1}{3}\{1 + p \mp 2[2p(1 - p)]^{1/2}\}. \tag{15b}$$

The results (14) and (15) can be easily deduced from the corresponding expressions for  $\epsilon_c$  as predicted by MGT and EMT, which in our notation, are given by

$$F(s)_{\text{MGT}} = \frac{p}{s - \frac{1}{3}(1 - p)} \tag{16}$$

$$F(s)_{\text{EMT}} = (1/4s) \{3s + 3p - 1 - [9s^2 - 6(1 + p)s + (1 - 3p)^2]^{1/2}\}. \tag{17}$$

It can be shown (Bergman 1978), that  $f(x)$  must satisfy certain sum rules, i.e.,

$$\int_{x_1}^{x_2} f(x) dx = p \tag{18}$$

$$\int_{x_1}^{x_2} xf(x) dx = \frac{1}{3}p(1 - p). \tag{19}$$

The first of these must always hold, whereas the second must hold if the system is isotropic or cubic. Both MGT and EMT satisfy these sum rules. In our model, the first sum rule is satisfied automatically. On the other hand, for any particular configuration we found that the second sum rule was usually violated by about 10%. This is easily understood once it is realised that the system does not in general have cubic point symmetry. Nevertheless, the continuous distribution  $f(x)$ , obtained by superimposing the poles of 60 different configurations never violated equation (19) by more than 2%. This indicates that the statistical average over the configurations leads to a system that is quite closely cubic or even isotropic.

Because they satisfy both sum rules, all of the theories provide similar predictions for  $\epsilon_c$  when  $s$  is far away from the region of nonanalyticity (e.g., when  $s$  is real and large, or  $s$  has a large imaginary part). In order to discriminate between the theories we must therefore look at values of  $s$  that are near the region of nonanalyticity, where the

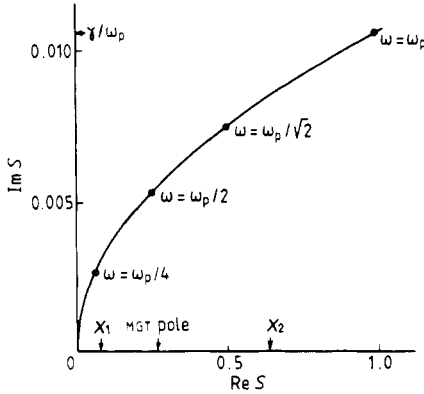


**Figure 2.** The trajectory of  $s(\omega)$  in the complex  $s$ -plane for  $0 < \omega < \omega_p$  for a hypothetical granular metal described in the text. Note the different length scales along the  $\text{Re } s$  and  $\text{Im } s$  axes. Note also that the scale of distance of the trajectory from the  $\text{Re } s$  axis is determined by the ratio  $\gamma/\omega_p$ .

predictions diverge. To illustrate this, consider the case of a hypothetical granular metal, made of metallic grains with a frequency dependent dielectric constant given by

$$\epsilon_1 = 1 - \frac{\omega_p^2}{\omega(\omega + i\gamma)} \tag{20}$$

inserted into an insulating matrix with  $\epsilon_2 = 1$ . Taking the plasma frequency to be  $\omega_p = 9.4 \times 10^{15} \text{ s}^{-1}$ , and the damping constant to be  $\gamma = 10^{14} \text{ s}^{-1}$ , we find

$$s = \frac{\omega(\omega + i\gamma)}{\omega_p^2} \tag{21}$$

In this case  $\gamma/\omega_p \ll 1$ . Part of the trajectory of  $s(\omega)$  in the complex  $s$ -plane is shown in figure 2. Clearly, for  $0 \leq \omega \leq \omega_p$  the trajectory passes close to the singular region. The location of the MGT pole and the branch points  $x_1$  and  $x_2$  of EMT are shown in the figure

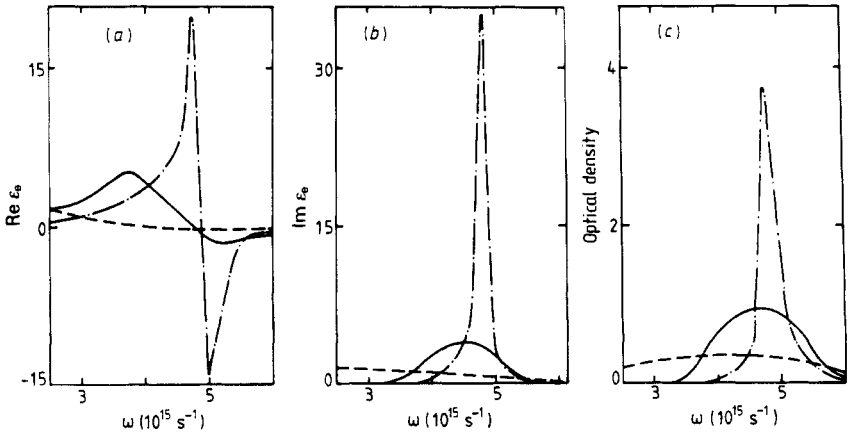


**Figure 3.** Graphs of (a)  $\text{Re } \epsilon_e$ , (b)  $\text{Im } \epsilon_e$  and (c) the optical density of the hypothetical granular metal (concentration  $p = 0.3$ ) as predicted by EMT (broken curve), MGT (chain curve) and our calculations (full curve).

for the case of metal concentration  $p = 0.3$ . In figure 3 we show  $\text{Re}\epsilon_e$ ,  $\text{Im}\epsilon_e$  and the optical density for this model, as predicted by MGT, EMT and our calculations. The differences among the various predictions can be easily understood with the help of figure 1: the whole weight of  $f(x)_{\text{MGT}}$  is concentrated at one point, which explains the sharp peak in figure 3;  $f(x)_{\text{EMT}}$  is broadly smeared, and thus predicts a very small and very broad peak;  $f(x)$  of our model looks like a somewhat broadened version of  $f(x)_{\text{MGT}}$ , and thus the peak predicted by our calculations is lower and broader.

### 3. Comparison with experiments

Any attempt to compare the theoretical predictions with the experimental results depends on a knowledge of the dielectric constant of the components. When we deal with metal grains inside an insulating matrix, the dielectric constant of the matrix is usually assumed to have its bulk value, which does not depend on the frequency in the frequency range that we are interested in. The bulk values of the dielectric constant of the metal are adapted to the case of small grains in the following way: the interband part of  $\epsilon$  is left unchanged, but in the free electron part of  $\epsilon$  the relaxation time  $\tau = 1/\gamma$  is adjusted so that the mean free path is equal to one half of the average grain size (Doyle 1958, Kawabata and Kubo 1966, Kreibig 1974).

In real materials that have been made, the differences between the predictions are smaller than in the hypothetical case discussed in the previous section, because the damping  $\gamma$  is much greater. Nevertheless there are considerable differences between the predictions of the different theories.

In figure 4 we show experimental and theoretical results for the optical density of a 30% Ag–70% SiO<sub>2</sub> mixture investigated experimentally by Cohen *et al* (1973). In plotting the theoretical graphs, we used  $\epsilon = 2.2$  for fused quartz (SiO<sub>2</sub>). For  $\epsilon(\omega)$  of Ag we used the form found by Johnson and Christy (1972) but, following Cohen *et al* (1973) we

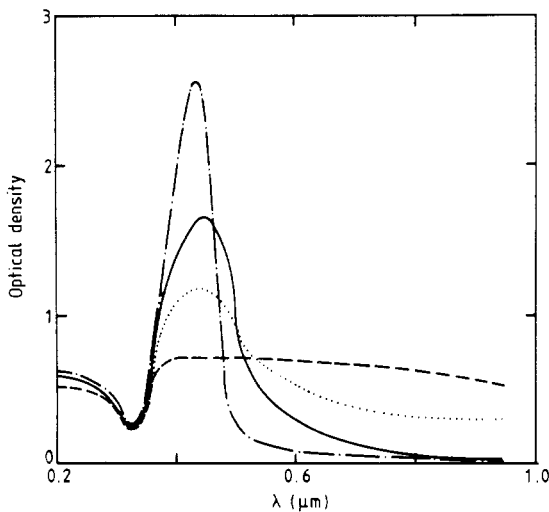


**Figure 4.** Optical density of 30% Ag–70% SiO<sub>2</sub> mixture as predicted by EMT (broken curve), MGT (chain curve) and our calculations (full curve). The experimental results (dotted curve) are taken from Cohen *et al* (1973). The thickness of the film is 640 Å.

replaced the bulk value of the relaxation time  $\tau$  by  $2.5 \times 10^{-15}$  s. This corresponds to a mean free path of about 25 Å, while the typical grain size is about 50 Å. The MGT and EMT graphs are similar to those drawn by Gittelman and Abeles (1977), i.e. EMT predicts no absorption peak, while MGT predicts a peak that is too high and narrow. Our model predicts a smaller and broader peak, but there is still some discrepancy between the predicted graph and the experimental results.

Although the peak we predict has the right position and width, it is still somewhat higher than the experimental peak. More disturbingly, at frequencies below the peak, the predicted absorption is too low. A possible reason for this could be that our model does not account correctly for the statistics of close approaches of individual grains. Earlier calculations on a periodic array of spherical inclusions (Bergman 1979b) lead to the qualitative conclusion that close approaches or clumping can be responsible for an enhancement of the absorption at low frequencies owing to the appearance of many resonances at small values of  $s$ .

Another possibility, which we cannot rule out at this time, arises from the fact that the experimental results in figure 4, taken from Cohen *et al* (1973), have actually been shifted somewhat arbitrarily by these authors so as to make them agree with MGT at a wavelength of 1  $\mu\text{m}$ . Therefore, the absolute values of the experimental optical density are known only to within a somewhat unknown additive constant.

As another example, we consider a 18% Mg–82%  $\text{MgF}_2$  mixture that was investigated experimentally by Sichel and Gittelman (1977). The experimental absorption curve is shown in figure 5, together with the predictions of EMT, MGT and our own calculation. The theoretical graphs were calculated using  $\epsilon = 1.96$  for  $\text{MgF}_2$ , while the  $\epsilon$  of Mg was taken from Hageman *et al* (1974), replacing the bulk value of  $\tau$  by the much smaller value  $\tau = 2.5 \times 10^{-16}$  s. This value corresponds to a mean free path of 4 Å, which would mean that each Mg grain consists of a few atoms. The actual grain size is not known in this case, but Sichel and Gittelman (1977) point out that there is a large number of very small grains in this mixture. The relaxation time can be viewed as an unknown adjustable parameter in this calculation: if we increase  $\tau$  the discrepancies between the theories

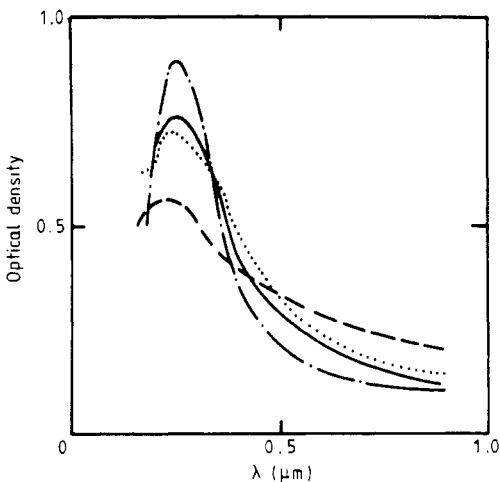


**Figure 5.** Optical density of an 18% Mg–82%  $\text{MgF}_2$  mixture as predicted by EMT (broken curve), MGT (chain curve) and our calculations (full curve). The experimental results (dotted curve) were taken from Sichel and Gittelman (1977). The thickness of the film is 600 Å.

and the experiment become greater. In this case MGT (EMT) predicts an absorption peak that is too strong (too weak). Our model predicts an absorption peak that is very close to the experimentally observed peak.

## 5. Summary and discussion

The dielectric constant  $\epsilon_c$  of a two component composite mixture can be expressed through the resonance density function  $f(x)$ , which depends only on the microgeometry of the mixture, and the dielectric constants of the components. We used a simple model to calculate  $f(x)$  for a composite with a special type of random geometry and the predictions that followed from this for the optical properties were in good agreement with experiments.

Among the simple theories, MGT seems to predict quite reasonably the optical properties of granular metals. The discrepancies between MGT and experiments indicate that  $f(x)_{\text{MGT}}$ , which is a  $\delta$ -function, is too sharp and therefore predicts an absorption peak that is too strong. On the other hand  $f(x)_{\text{EMT}}$  seems to be too broad. Most attempts to obtain an improved expression for  $f(x)$  were made in two directions: (i) introduction of randomness in the grain shapes, such as randomly oriented ellipsoids (Polder and van Santen 1946, O'Neill and Ignatiev 1978) and (ii) attempts to take into account higher order interactions between the grains, e.g. a calculation of polarisabilities of grain clusters (Yoshida *et al* 1971, Meessen 1972, Bedeaux and Vlieger 1974, Vlieger 1979) or direct introduction of effective polarisabilities (Granqvist and Hunderi 1978a, b) and subsequent use of these polarisabilities in EMT or MGT.

Our calculation demonstrates that the  $\delta$ -function peak of  $f(x)_{\text{MGT}}$  can be broadened merely by taking into account the disorder in the locations and radii of individual spheres (without introducing any disorder in the shapes), and by and taking into account the higher order interactions between different spheres. It seems as though by increasing the number of spheres in our repeated cubic cell and by taking into account still higher order interactions we should be able to get even better agreement with experiments.

Finally, it should be noted that since the entire calculation is based upon the static approximation to Maxwell's equations (this is true also of MGT and EMT), it is bound to fail if  $\omega$  is large enough. However, as long as the grain size is much less than the wavelength of the electromagnetic waves and the skin depth, the static approximation is expected to be good.

## Appendix

The matrix element in equation (11) is the sum of the overlap integrals between the  $(l, m)$  state of the  $i$ th grain in one cell and the  $(l', m')$  states of  $j$ th grains in all the cells. The vector separation between the two grains is expressed in the form

$$\mathbf{r} = (r, \theta, \varphi) = \mathbf{R}_0 + \mathbf{r}_j - \mathbf{r}_i \equiv \mathbf{R}_0 + \mathbf{r}' \equiv (R_0, \theta_0, \varphi_0) + (r', \theta', \varphi') \quad (\text{A1})$$

where  $\mathbf{r}_i$  and  $\mathbf{r}_j$  are the locations of the  $i$ th and  $j$ th grains in the same unit cell, while  $\mathbf{R}_0$  is the separation between the two unit cells containing the grains  $i, j$ . Thus the matrix element given by equation (10) should be summed over all lattice vectors  $\mathbf{R}_0$  (including  $\mathbf{R}_0 = 0$ ). The last term in equation (11) is the  $\mathbf{R}_0 = 0$  term of the sum. We are left with the summation only over non-zero lattice vectors. The matrix element of equation (10),

which depends on the intergrain separation  $r$ , is expanded in a sum of products of a function of  $r'$  and a function of  $\mathbf{R}_0$  (this is done with the help of results from Danos and Maximon (1965), as described by Bergman (1979a))

$$\frac{P_L^M(\cos \theta) \exp(iM\varphi)}{r^{L+1}} \sum_{\lambda=0}^{\infty} \sum_{\mu=-\lambda}^{\lambda} (-1)^{\lambda+\mu} \frac{(L+\lambda+\mu-M)!}{(\lambda+\mu)!(L-M)!} r'^{\lambda} P_{\lambda}^{\mu}(\cos \theta') \exp(i\mu\varphi') \\ \times \frac{P_{L+\lambda}^{M-\mu}(\cos \theta_0) \exp[i(M-\mu)\varphi_0]}{R_0^{L+\lambda+1}}. \quad (\text{A2})$$

This expression may now be summed over the non-zero lattice vectors  $\mathbf{R}_0$ , and that leads to a factor  $\sigma(L+\lambda, |M-\mu|)$ , as defined earlier in equation (13). Replacing  $(L, M)$  by  $(l+l', m'-m)$  in equation (A2), and omitting the primes in  $(r', \theta', \varphi')$ , we finally arrive at equation (11).

## References

- Bedeaux D and Vlieger J 1974 *Physica* **73** 287  
 Bergman D J 1978 *Phys. Rep.* **43** 377  
 ——— 1979a *Phys. Rev. B* **19** 2359  
 ——— 1979b *J. Phys. C: Solid State Phys.* **12** 4947  
 Bruggeman D A G 1935 *Ann. Phys. Lpz.* **24** 636  
 Cohen R W, Cody G D, Coutts M D and Abeles B 1973 *Phys. Rev. B* **8** 3689  
 Danos M and Maximon L C 1965 *J. Math. Phys.* **6** 766  
 Doremus R H 1964 *J. Chem. Phys.* **40** 2389  
 ——— 1965 *J. Chem. Phys.* **42** 414  
 Doyle W J 1958 *Phys. Rev.* **111** 1067  
 Gittelmann J I and Abeles B 1977 *Phys. Rev. B* **15** 3273  
 Granqvist C G, Buhrman R A and Wyns J 1976 *Phys. Rev. Lett.* **37** 625  
 Granqvist C G, Calander N and Hunderi O 1979 *Solid State Commun.* **31** 249  
 Granqvist C G and Hunderi O 1978a *Phys. Rev. B* **18** 1554  
 ——— 1978b *Phys. Rev. B* **18** 2897  
 Hageman H J, Audat W and Kuntz C 1974 *Optical Constant from the Far Infrared X-ray Region: Mg, Al, Cu, Ag, Au, Bi, C and Al<sub>2</sub>O<sub>3</sub>* (Hamburg: DESY)  
 Ignatiev A, O'Neill P, Doland C and Zajac G 1979 *Appl. Phys. Lett.* **34** 42  
 Jarrett D N and Ward L 1976 *J. Phys. D: Appl. Phys.* **9** 1515  
 Johnson P B and Christy R W 1972 *Phys. Rev. B* **19** 4370  
 Kawabata A and Kubo R 1966 *J. Phys. Soc. Japan* **21** 1865  
 Kreibitz U 1974 *J. Phys. F: Met. Phys.* **4** 999  
 Landauer R 1952 *J. Appl. Phys.* **23** 779  
 Lissberger P H and Nelson R G 1974 *Thin Solid Films* **21** 159  
 Maxwell-Garnett J C 1904 *Phil. Trans. R. Soc.* **203** 385  
 ——— 1905 *Phil. Trans. R. Soc.* **205** 237  
 Meessen A 1972 *J. Physique* **33** 371  
 Messiah A 1962 *Quantum Mechanics* (Amsterdam: North-Holland) pp 492–6  
 Norman S, Andersson T, Granqvist C G and Hunderi O 1978 *Phys. Rev. B* **18** 674  
 O'Neill P and Ignatiev A 1978 *Phys. Rev. B* **18** 6540  
 Polder D and van Santen J H 1946 *Physica* **12** 257  
 Sheng P 1980a *Phys. Rev. Lett.* **45** 60  
 ——— 1980b *Phys. Rev. B* **22** 6364  
 Sichel E K and Gittelmann J I 1977 *RCA Lab. Rep.* May 1977  
 Tanner D B, Sievers A J and Buhrman R A 1975 *Phys. Rev. B* **11** 1330  
 Vlieger J 1979 *Physica* **64** 63  
 Yoshida S, Yamaguchi T and Kinbara A 1971 *J. Opt. Soc. Am.* **61** 62